

Relaxation of stationary states on a quantum computer yields a unique spectroscopic fingerprint of the computer's noise

Scott E. Smart¹, Zixuan Hu², Sabre Kais² & David A. Mazziotti¹  [✉]

Quantum computing has the potential to revolutionize computing, but its significant sensitivity to noise requires sophisticated error correction and mitigation. Traditionally, noise on the quantum device is characterized directly through qubit and gate measurements, but this approach has drawbacks in that it does not adequately capture the effect of noise on realistic multi-qubit applications. In this paper, we simulate the relaxation of stationary quantum states on a quantum computer to obtain a unique spectroscopic fingerprint of the computer's noise. In contrast to traditional approaches, we obtain the frequency profile of the noise as it is experienced by the simulated stationary quantum states. Data from multiple superconducting-qubit IBM processors show that noise generates a bath within the simulation that exhibits both colored noise and non-Markovian behavior. Our results provide a direction for noise mitigation but also suggest how to use noise for quantum simulations of open systems.

¹Department of Chemistry and The James Franck Institute, The University of Chicago, Chicago, IL 60637, USA. ²Department of Chemistry, Department of Physics, and Purdue Quantum Science and Engineering Institute, Purdue University, West Lafayette, IN 47907, USA. ✉email: [damazz@uchicago.edu](mailto:damaz@uchicago.edu)

Quantum computing, as conceived by Feynman¹, has the potential to revolutionize computing for certain classes of problems with exponential scaling in the physical and social sciences and engineering^{2–10}. Central to the quantum computing paradigm is the quantum process of entanglement by which a pure-state quantum system develops a probability distribution over multiple classical outcomes. Entanglement allows us to process and store exponentially more information than a classical computer. This potential capability and its advantages, however, come with a significant sensitivity to noise^{6,11–13} that introduces errors that degrade performance, especially on current-to-near-term quantum computers. Significant advances have been made in the past decade in error correction and mitigation^{14–19}, but further advances are needed to not only understand noise but also control noise for its mitigation or exploitation.

In quantum mechanics, a closed system which is in a stationary state will remain in that state for all time. If, however, the closed quantum system is opened to an environment, also referred to as a bath, then the system becomes an open-quantum system, and a stationary state of that system will potentially become time-dependent and non-stationary¹¹. The precise time dependence of the open quantum system depends upon the nature of the bath. If the relaxation of the bath is fast relative to the dynamics of the system, then the quantum dynamics is purely dissipative and described as Markovian, but if the dynamics of the bath and system are on the same timescale, then the dynamics causes energy to be exchanged both to and from the bath and is described as non-Markovian^{11,13,20}. In non-Markovian dynamics the more complex interaction between the system and bath causes the system to develop a memory of its state as a function of time.

We can broadly characterize noise or the effects of noise through spectroscopic or tomographic techniques. In the context of quantum computing, characterization of the bath, which is commonly assumed to be Markovian, gives a basic assessment of the qubit and gate performance. While quantum process tomographic techniques can be used^{21–24}, they are costly and potentially unreliable for realistic measurement, and other alternatives such as randomized benchmarking or quantum gate set tomography have emerged as more robust tools^{25–27}. Non-Markovian behavior is present in a variety of systems, but is generally more challenging to characterize^{28,29}. Efficient characterization of an underlying interaction is also possible for one or two-qubit systems^{30,31}. In the frame of a simulated quantum system, however, we are not usually concerned with the characterization of the device, but the bath in relation to the simulated system.

In this paper, we simulate stationary states on a quantum computer to obtain a unique spectroscopic fingerprint of the computer's noise. If a quantum system in a stationary state is simulated on an ideal quantum computer, the quantum system will remain in that stationary state for all time. However, if the same system is simulated on a noisy intermediate-scale quantum (NISQ) computer, the noise causes the simulated state to become non-stationary. The resulting time dependence in the frame of the simulation provides us with a frequency profile of the noise as it is experienced by the simulated stationary quantum state. Knowledge of the bath in the frame of the simulated system can potentially be utilized in the simulation of other noisy quantum systems or the design of better algorithms for quantum simulations^{32,33}. Computations are performed on multiple superconducting-qubit IBM quantum computers. We find that each quantum computer has a unique spectroscopic signature for a given simulation of stationary states. The noise generates an effective bath that exhibits both colored noise and non-Markovian behavior^{11,13,20}. Characterization of the bath provides an application-oriented assessment of the fidelity of the

quantum device. Our results provide a direction for noise mitigation but also suggest how to use noise for quantum simulations of open systems^{8,34–41}.

Results

Stationary-state evolution with noise. Time evolution of a stationary state prepared on a noisy quantum computer can be described by the equation of motion of the density matrix D according to the Nakajima–Zwanzig integro-differential equation^{11,13,42}

$$\frac{dD}{dt} = -\frac{i}{\hbar}[\hat{H}, D] + \int_0^t \mathcal{K}(t, \tau)D(t, \tau)d\tau, \quad (1)$$

where \hat{H} is the Hamiltonian operator of the stationary state and $\mathcal{K}(t, \tau)$ is the memory kernel representing the quantum computer's noise. The memory kernel as represented here also includes the contribution of memoryless (i.e., Markovian) noise effects, which can be represented by a Dirac delta function at t in the kernel. In the limit that the noise on the quantum computer vanishes, the memory kernel vanishes and the equation simplifies to the quantum Liouville (von Neumann) equation. If the initial state is a stationary state of \hat{H} , all of the non-trivial time dependence results from the noise. Normal noise spectroscopy or characterization of a system could be performed by using a number of techniques, such as with Rabi spectroscopy, swap spectroscopy, or with a tunable system^{43–51}. Here, to probe the frequency dependence of the noise, we consider the family of scaled Hamiltonians $\hat{H} = \hbar\omega\hat{O}$ where \hat{O} is a dimensionless operator. By changing ω , we can control the energy difference between the ground and the first excited state of the simulated system. The time-dependent response of the system to different values of ω provides us with spectral information about the noise on the quantum computer. From one perspective we are attempting to simulate the solution of the quantum Liouville equation on the quantum computer with the memory kernel set to zero. Consequently, all deviations from the closed-system evolution are originating from the noise of the given quantum computer which creates without our direction an effective memory kernel for the time evolution (including memoryless effects).

Single-qubit Hamiltonians. We begin with a single-qubit system with the Hamiltonian matrix $H(\omega) = \omega\sigma_z$ where we use atomic units with $\hbar = 1$, and σ_z is the Pauli-Z matrix,

$$\sigma_z = \begin{pmatrix} 1 & 0 \\ 0 & -1 \end{pmatrix}. \quad (2)$$

We prepare the system in the excited state $|\psi\rangle = |1\rangle$ and evolve the system according to $\exp[-iH\tau] = R_z(2\omega\tau)$, using repeated single-qubit gates with the results shown in Fig. 1. The time step is arbitrary to the extent that it can be rescaled with the strength of the Hamiltonian (in this case, ω), and hence, we set $\tau = \frac{1}{3}$, which serves to highlight system-bath interactions when the frequency $\omega \in [0, 1]$. If we allowed the system to relax without applying any gates, this would essentially be a T_1 experiment (where we could use the physical gate times), measuring the relaxation time for an excited state. However, the noise sources here, represented by the non-vanishing memory kernel, generate non-Markovian behavior. In Fig. 1, the non-Markovian behavior can be seen from the oscillations in the population of the ground state, which reveal a memory dependence beyond the pure decay of Markovian dynamics. Furthermore, the oscillations are more pronounced at lower frequencies, indicating a bath with colored noise.

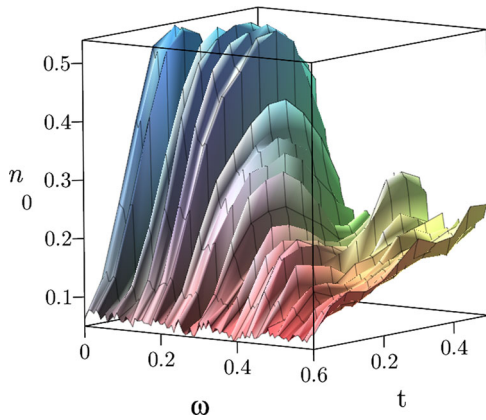


Fig. 1 Frequency scan of simulated time evolution for a single qubit. Scan of population of the $|0\rangle$ state (n_0) as a function of simulated time t and frequency ω on the ibmq_armonk device. We initially prepare the $|1\rangle$ state and then apply 100 total gate sequences of $\exp[-i\tau H]$, where the time step is $\tau = \frac{1}{3}$, the system Hamiltonian is $H = \omega\sigma_z$, $\omega \in (0, 0.6)$, and σ_z is defined in Eq. (2). The time t is equal to the number of gates times τ multiplied by the scaling factor 0.015. The oscillatory behavior reveals non-Markovian effects with the oscillations becoming less pronounced at higher frequencies.

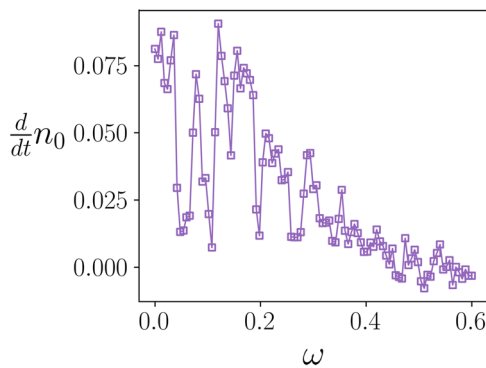


Fig. 2 Rate of population change with respect to simulated time for different frequencies with a single-qubit system. Approximate rate of ground-state populations changes $\frac{d}{dt}n_0$ as a function of frequency ω evaluated after the first time step, which is proportional to the spectral density. The data is taken from the scan in Fig. 1 from ibmq_armonk.

The spectral density with respect to a quantum noise source A can be characterized as⁴⁹:

$$S_A(\omega) = \int_{-\infty}^{\infty} d\tau \exp[i\omega\tau] \sum_{\alpha\beta} \rho_{\alpha\alpha} \langle \alpha | A(\tau) | \beta \rangle \langle \beta | A(0) | \alpha \rangle \quad (3)$$

$$= 2\pi \sum_{\alpha,\beta} \rho_{\alpha\alpha} |A_{\alpha\beta}|^2 \delta(\epsilon_\beta - \epsilon_\alpha - \omega),$$

where α and β are energy eigenstates of H and ρ represents the density matrix. The spectral density can be related to the rate of population change through first-order perturbation theory with the well-known Fermi's golden rule^{12,49,52}. Figure 2 is constructed from Fig. 1, showing the rate of change in the initial part of the time evolution as a function of frequency, which provides a rough spectrum of the noise on the quantum computer from the perspective of the simulated system. Note that for frequencies above 0.6 (relative to a value of $\tau = 1/3$), the noise profile shows low-intensity signals, likely from thermal noise. The appropriate resolution is difficult to determine, and the wells are not stochastic, as a purely stochastic phenomenon would not be

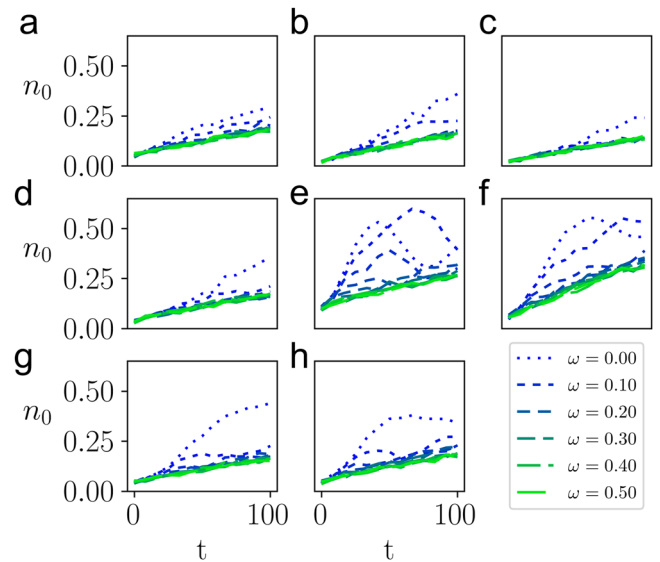


Fig. 3 Demonstration of simulated time evolution for different devices and qubits. Ground-state populations n_0 obtained from simulated time evolution with different devices and qubits (indicated by the i th qubit Q_i). Systems were initialized in the $|1\rangle$ state and evolved for time t with Hamiltonian $H = \omega\sigma_z$. The frequency is given by ω , time step $\tau = \frac{1}{3}$, and σ_z defined in Eq. (2). **a** Q2, ibmq_belem. **b-d** Q0, Q2, Q4, ibmq_bogota. **e** Q0, ibmq_armonk. **f-h** Q0, Q2, Q4, ibmq_casablanca. Legend shows frequencies ranging from $\omega = 0$ (blue, shortest dashes) to $\omega = 0.5$ (green, longest dashes).

continuous along the time series since each time in the series is sampled independently.

The significant portion of the noise can be ascribed to a transverse noise source (described by the Pauli-X or -Y matrices) which allows for transitions between the ground and excited states. The quantum devices we studied utilize a sequence of elementary gates denoted as U_1 , U_2 , and U_3 gates. In particular, these gates consist of alternating frame changes (R_z gates) and rotations ($X90$ rotation, R_x gates), where U_k contains k frame changes and $k - 1$ transverse rotations (in the current iteration of IBM systems, these gates are represented with a series of intertwined R_z and \sqrt{X} gates, which can also be used in a similar manner to represent generic single-qubit unitary transformations). If only the U_1 gate is used to model $\exp[-i\omega\sigma_z\tau]$, then a pulse is not applied, and the gate applications correspond to a standard T_1 experiment, measuring the relaxation of the excited state. However, here we specifically use U_3 gates, which are generic single-qubit rotations, and which alternate between transverse and longitudinal rotations. In fact, one way to model similar behavior in the qubit system is to apply a constant $\exp[i\theta\sigma_x]$, where θ is taken to be a small angle, following every gate application. However, this does not account for the troughs seen within the range from 0.03 to 0.3. Whether or not the noise channels are a result of an improper calibration of the $X90$ gate resulting in a systematic overrotation, or are part of a completely different noise source, becomes irrelevant for the noisy system in that the quantum system could be equivalently described from either perspective^{45,53}. For a user or algorithm that does not control the qubit and gate level of the simulation, we posit that the effects of the two are the same, and the quantum system could be viewed as experiencing the same.

In addition to using different devices, we also can highlight system-specific responses on a single device by choosing different qubits to simulate our system. We demonstrate this in Fig. 3. In Fig. 3a, b, c, d, it appears that only one or two frequencies in the

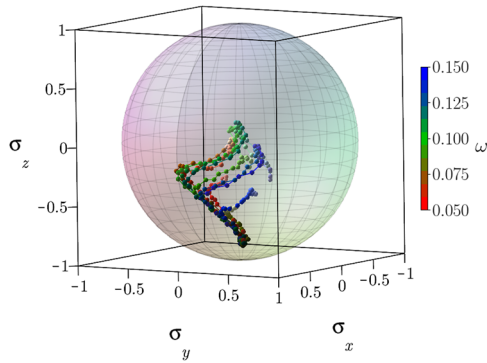


Fig. 4 Single-qubit state trajectories with respect to simulated time for a range of frequencies. Scan of several trajectories represented in the Bloch sphere for a single-qubit device for a range of frequencies $\omega \in [0.05, 0.15]$ in increments of 0.01, from `ibmq_armonk`. σ_i represents the expectation with respect to that operator as a function of time. Each simulation has an equal number of gate applications and changes only the frequency ω in the propagation with time step τ , $\exp[-i\tau H] = \exp[-i\frac{\omega\sigma_z}{3}]$. ω decreases from red ($\omega = 0.05$) to green ($\omega = 0.10$) to blue ($\omega = 0.15$).

simulated evolution show a frequency-dependent response, which in some instances appears to be Markovian. However, for others, like in Fig. 3e, f, g, h we see strong non-Markovian behavior at numerous frequencies. The highest frequencies in each case appear to exhibit simple exponential decay, and so can be taken as an indicator of the simulated relaxation time. Note that a strict comparison cannot be made between the simulated relaxation time and the qubit performance characteristics. For single qubit with high-fidelity gates, we might expect the T_1 time to mirror the simulated relaxation rate (see Supplementary Note I for an explicit comparison). In practice, however, gate errors obfuscate the comparison by contributing to the simulated relaxation rates. Also, the evolution by gate applications introduces energy into the system, which causes the system to relax into a mixed ensemble state rather than the ground state.

We can also observe how the quantum state vector moves in the Bloch sphere at different frequencies. For frequencies in the high region of the spectral density and not allowing for coupling between the bath and system, a slow precession around the axis corresponding to H is observed. However, for frequencies which couple to the bath, the system can be strongly pulled around the Bloch sphere resulting in various trajectories through the state space. We model some of the trajectories in Fig. 4, and instances with other Hamiltonians are included in Supplementary Note I.

Two-qubit Hamiltonians. By identifying frequencies of interest on the qubits themselves, we can construct systems which respond uniquely to the bath, allowing for selective transitions between different eigenstates of the system. With this in mind, we first simulate a two-qubit system with a local Hamiltonian defined by:

$$H(\omega_1, \omega_2) = \omega_1 \sigma_z^1 + \omega_2 \sigma_z^2. \tag{4}$$

where σ_z^j refers to the Pauli-Z matrix in Eq. (2) acting on the j th qubit. This Hamiltonian has the computational basis as its energy eigenbasis, and it can be shown that changing a frequency ω_i can lead to a small energy transition between states differing locally on qubit i . By scanning over single-qubit frequencies, we can obtain a simple noise profile, and then choose appropriate ω_i to influence the system. Using these frequencies, we highlight four different cases in Fig. 5a, b, c, d, showing interacting and non-interacting frequencies for each qubit. In addition, we present the calculated transition rates for each population in Table 1.

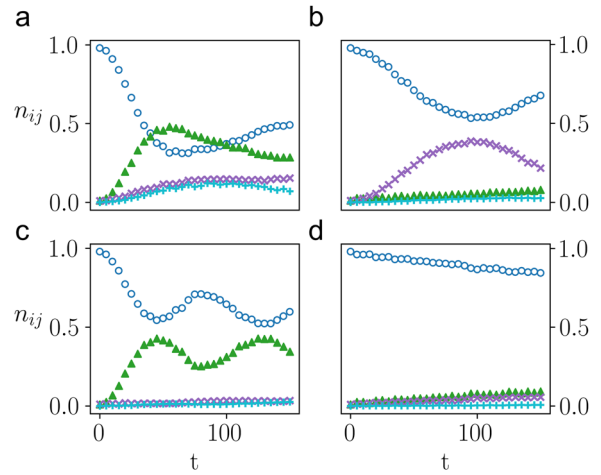


Fig. 5 Simulated time evolution of a two-qubit local system which demonstrates state transitions on local sites. Populations n_{ij} where $i, j \in \{0, 1\}$, referring to the eigenstates of the two-qubit system undergoing simulated evolution for time t with time step $\tau = 1/3$ prepared on `ibmq_rome`. The system Hamiltonian can be described with two frequencies: $H(\omega_1, \omega_2) = \omega_1 \sigma_z^1 + \omega_2 \sigma_z^2$ where σ_z^i on qubit i is given by Eq. (2). The different plots describe permutations of two different values of ω_1 and ω_2 . **a** $(\frac{1}{20}, \frac{1}{20})$; **b** $(\frac{1}{20}, \frac{1}{2})$; **c** $(\frac{1}{2}, \frac{1}{20})$; **d** $(\frac{1}{2}, \frac{1}{2})$. Note that the bath is not symmetric with respect to the swapping of the qubits, as there is a stronger interaction of the bath with the second qubit relative to the first qubit. The populations are represented as n_{00} : \circ (blue), n_{01} : \triangle (green), n_{10} : \times (purple), and n_{11} : $+$ (cyan).

		$\frac{d}{dt} n_{ij} (\times 10^{-3})$			
ω_1	ω_2	n_{00}	n_{01}	n_{10}	n_{11}
$\frac{1}{20}$	$\frac{1}{20}$	-16.4	12.4	2.5	1.5
$\frac{1}{20}$	$\frac{1}{2}$	-4.7	0.5	4.1	0.2
$\frac{1}{2}$	$\frac{1}{20}$	-13.7	13.5	0.0	0.2
$\frac{1}{2}$	$\frac{1}{2}$	-1.1	0.7	0.4	0.0

Rate of population change for eigenstates n_{ij} , where ij are indices (corresponding to the computational basis), immediately after initialization for the two-qubit system depicted in Fig. 5, where $H = \omega_1 \sigma_z^1 + \omega_2 \sigma_z^2$, time step $\tau = \frac{1}{3}$ and σ_z^i on qubit i is given by Eq. (2). The rate was averaged over 15 time steps. The strongest bath interaction is related to a small frequency ω_1 , which when isolated or in conjunction with ω_2 has strong enough coupling to induce state transitions. The only significant increase in the n_{11} state occurs when a low transition frequency is available for both qubits. In addition, these rates are substantially lower than what is observed in the single-qubit system, which corresponds with the better gate fidelities for this system (see Supplementary Note II).

The system here demonstrates asymmetry between the two qubits, with stronger coupling present on the second qubit. For large ω_1 and ω_2 , which do not strongly couple the bath and qubit system, we witness a region of linear decay toward a uniformly depolarized state. For smaller ω_1 and ω_2 , we clearly have a very dynamic system, allowing for transitions amongst all four states.

We can expand this idea naturally to look at a potentially non-local Hamiltonian, namely:

$$H(\omega_1, \omega_2, \omega_3) = \omega_1 \sigma_z^1 + \omega_2 \sigma_z^2 + \omega_3 \sigma_z^1 \sigma_z^2. \tag{5}$$

The time propagator for this step is still relatively simple, as all elements commute and there is no Trotterization error. In addition, the eigenstates correspond to elements of the computational basis. Practically, the propagator requires only 2 CNOT gates with a sequence of exponential Z rotations. If we consider

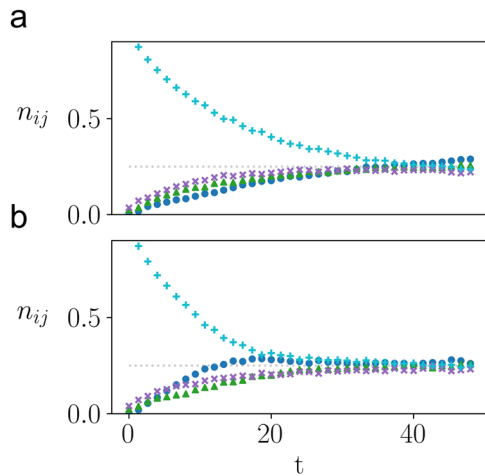


Fig. 6 Demonstration of a $|11\rangle \rightarrow |00\rangle$ eigenstate transition in the simulated time evolution of a correlated two-qubit system. Simulated evolution for time t on ibmq_bogota where the time step $\tau = 1/3$, and the Hamiltonian is composed of three variable frequencies ω_i , $\hat{H} = \omega_1\sigma_x^1 + \omega_2\sigma_x^2 + \omega_3\sigma_x^1\sigma_x^2$, where σ_x^i acting on qubit i is given by Eq. (2). **a** Using $\omega_3 = 1$, and $\omega_1, \omega_2 = \frac{1}{2}$, the system demonstrates expected exponential decay to the thermally mixed state. **b** With $\omega_3 = 1$ and frequencies, $\omega_1 = \frac{1}{10}$ and $\omega_2 = -\frac{1}{20}$, despite the quick decay we see a correlated two-qubit transition between the $|11\rangle$ and $|00\rangle$ eigenstates where the other populations match the decay seen in **(a)**. The dotted grey line represents the ideal fully mixed population for each eigenstate $n_{ij} = \frac{1}{4}$. The simulated populations are represented as n_{00} : \circ (blue), n_{01} : \triangle (green), n_{10} : \times (purple), and n_{11} : $+$ (cyan).

the eigenstate state with density matrix $\rho_0 = |11\rangle\langle 11|$, we can elucidate information on the eigenstates and relative differences between states. Given the Hamiltonian above, we can describe state-to-state transitions with energy gaps given by:

$$\epsilon_{00} - \epsilon_{11} = 2(\omega_1 + \omega_2) \quad (6)$$

$$\epsilon_{01} - \epsilon_{11} = 2(\omega_1 - \omega_3) \quad (7)$$

$$\epsilon_{10} - \epsilon_{11} = 2(\omega_2 - \omega_3). \quad (8)$$

For local Hamiltonians, transitions from the $|11\rangle$ state are predominantly induced by local transitions ($\epsilon_{00} - \epsilon_{11}$ for Eq. (4) is $\omega_1 + \omega_2$, and so if ω_1 and ω_2 are small we can induce other transitions simultaneously). For this correlated Hamiltonian we can independently control energy levels, and thus have more control over the available transitions. However, we also know that noise from multi-qubit gates will be stronger, resulting in a quicker decay process. Figure 6 shows simulated evolution for two sets of frequencies demonstrating different potential behaviors which the system exhibits in response to the bath. The evolution here involves 144 time steps, or 288 CNOT gates, which can be seen to eventually lead to a fully mixed state where each population is $\sim 1/4$. In Fig. 6a, we choose frequencies that do not demonstrate a particular bath response, i.e., a large ω_3 , ω_1 , and ω_2 . As a result the system displays exponential decay. In Fig. 6b, we choose a large ω_3 with small values of ω_1 and ω_2 , which in principle allows for a correlated transition from the $|11\rangle$ eigenstate to the $|00\rangle$ eigenstate. Despite the presence of a stronger bath, we still see a transition between these eigenstates. When comparing the simulations in Fig. 6a and b, the $|00\rangle$ and $|11\rangle$ populations differ along the simulated trajectory by 0.13 and 0.12, respectively, whereas the $|01\rangle$ and $|10\rangle$ populations differ by only 0.028 and 0.023, respectively. Thus, we demonstrate that we can characterize the unique system-bath behavior of a correlated simulated quantum system.

Conclusions. By characterizing noise properties of the system, we may be able to design better error mitigation techniques or approaches to the simulation of open quantum systems where the quantum computer's noise is harnessed as an effective bath³². For example, examining the spectral profile of the bath from the simulation of stationary quantum states may provide a unique spectroscopic fingerprint of the quantum computer. With such a fingerprint we may be able to design simulation algorithms that account for this fingerprint, providing a potentially elegant approach to error mitigation for real-world applications. Furthermore, there may be certain scenarios such as open-quantum-system simulation where the presence of noise may be a beneficial quantum resource. This idea was recently demonstrated for qubit-like spin radical systems with the decoherence of qubits being utilized³³. To model an open-quantum system, we may be able to use the quantum computer's noise to represent a significant part of the model's bath. Use of the quantum computer's inherent noise could potentially permit the simulation of an open quantum system at a significantly reduced computational cost in terms of both gate and qubit resources. The present approach also provides insights into controlling noise relative to a simulated timescale. Similar to extrapolation schemes for error mitigation⁵⁴, we could use knowledge of the bath interaction to manipulate the noise strength as a function of the propagation step in time.

In addition, although noise sources in driven evolution cannot typically be attributed to singular sources, the absence of such specificity is not necessarily an issue for practical quantum computing. As mentioned above, characterizing whether the transverse signal is a systematic overrotation or an errant noise source is critical in calibration but not so important for system applications. For a complex quantum simulation, the effects of a single source of error (unless uniquely distinct) cannot be easily distinguished amidst the entire chorus of noise sources. From the complex set of instructions on a quantum computer emerges a complex noise profile, which is manifest in the difficulty of simulating multi-qubit noise phenomena. Through a simulated system-specific approach, we can utilize the effective bath's spectroscopic information to design more device-specific techniques and algorithms that could improve future applications.

In this work, we simulate the time evolution of arbitrary stationary quantum states on a noisy quantum computer through the application of the time evolution operator. Noise causes a system-specific response which exhibits Markovian and non-Markovian behaviors for certain frequency domains. Spectroscopic analysis of this time evolution provides a frequency spectrum—a spectroscopic fingerprint—of the noise of the effective bath induced by the quantum computer. Understanding the noise profile may allow us to create parameterized systems in which we influence state transitions with the quantum device serving as a non-Markovian bath. The characterization of the bath is shown to be robust through simulations on multiple IBM superconducting-qubit quantum computers with different qubit numbers, connectivities, and fidelities. Although the present work employs superconducting-qubit quantum computers, in future work we plan to use this approach to characterize the noise on other types of quantum computers such as ion-trap quantum devices. These ideas provide a further step toward harnessing the unique quantum noise profile which emerges from the perspective of a simulated system on a quantum computer, that could be utilized in approaches for error mitigation and the simulation of open quantum systems.

Methods

In each simulation we use atomic units, and the time steps are relative to meaningful scales on the quantum device. While we could associate the results to a physical time through the known gate lengths, we focus on presenting the time

evolution from the perspective of the simulated system, which can have arbitrary energies and time values, and which ultimately is beholden to the gate errors. As mentioned in the text, the system Hamiltonian has a single qubit or in the two-qubit system, a sum of two-single-qubit gates, both of which can be implemented as exact exponentials. These are implemented with U_3 gates on the quantum computer, which have the form:

$$U_3(\theta, \phi, \lambda) = R_z(\phi)R_x\left(-\frac{\pi}{2}\right)R_z(\theta)R_x\left(\frac{\pi}{2}\right)R_z(\lambda) \quad (9)$$

$$= \begin{pmatrix} \cos\left(\frac{\theta}{2}\right) & -e^{i\lambda}\sin\left(\frac{\theta}{2}\right) \\ e^{i\phi}\sin\left(\frac{\theta}{2}\right) & e^{i(\phi+\lambda)}\cos\left(\frac{\theta}{2}\right) \end{pmatrix}. \quad (10)$$

In preparing the manuscript, the user-input basis gate sequence for the ibmq devices was updated, so that now the U_3 transformation is implemented as a series of 3 R_z gates interleaved with \sqrt{X} gates (using the identity $R_x\left(\frac{\pi}{2}\right) = e^{-\frac{\pi}{4}}\sqrt{X}$). The correlated two-qubit example requires 2 CNOT gates in addition to the U_3 sequences.

Each circuit (representing a particular time point) is prepared by evolving in time according to the given time step, and then measuring the particular step 2^{13} times. Sampling errors throughout are smaller than the depicted markers. The simulations use cloud-available quantum devices accessible through IBM Quantum Experience. The particular results reported here are performed on ibmq_armonk, ibmq_rome, ibmq_beleg, ibmq_casablanca, and ibmq_bogota. The devices use fixed-frequency transmon qubits with co-planar waveguide resonators^{55,56}. We use the Python package Qiskit (v0.17.0)⁵⁷ to interface with the device. Specific device properties relevant to each run can be found in Supplementary Note II.

Data availability

The data generated during the current study are available from the corresponding author on reasonable request.

Code availability

Code will be made available on a public Github repository upon publication.

Received: 3 May 2021; Accepted: 22 December 2021;

Published online: 25 January 2022

References

- Feynman, R. P. Simulating physics with computers. *Int. J. Theor. Phys.* **21**, 467–488 (1982).
- Abrams, D. S. & Lloyd, S. Quantum algorithm providing exponential speed increase for finding eigenvalues and eigenvectors. *Phys. Rev. Lett.* **83**, 5162 (1999).
- Lloyd, S. Universal quantum simulators. *Science* **273**, 1073 (1996).
- Kandala, A. et al. Hardware-efficient variational quantum eigensolver for small molecules and quantum magnets. *Nature* **549**, 242 (2017).
- McArdle, S., Endo, S., Aspuru-Guzik, A., Benjamin, S. C. & Yuan, X. Quantum computational chemistry. *Rev. Mod. Phys.* **92**, 015003 (2020).
- Head-Marsden, K., Flick, J., Ciccarino, C. J. & Narang, P. Quantum information and algorithms for correlated quantum matter. *Chem. Rev.* <https://doi.org/10.1021/acs.chemrev.0c00620> (2020).
- Farhi, E., Goldstone, J. & Gutmann, S. A quantum approximate optimization algorithm. Preprint at <https://arxiv.org/abs/1411.4028> (2014).
- Hu, Z., Xia, R. & Kais, S. A quantum algorithm for evolving open quantum dynamics on quantum computing devices. *Sci. Rep.* **10**, <https://doi.org/10.1038/s41598-020-60321-x> (2020).
- Sager, L. M., Smart, S. E. & Mazziotti, D. A. Preparation of an exciton condensate of photons on a 53-qubit quantum computer. *Phys. Rev. Res.* **2**, <https://doi.org/10.1103/physrevresearch.2.043205> (2020).
- Smart, S. E. & Mazziotti, D. A. Quantum solver of contracted eigenvalue equations for scalable molecular simulations on quantum computing devices. *Phys. Rev. Lett.* **126**, <https://doi.org/10.1103/physrevlett.126.070504> (2021).
- Breuer, H. P. & Petruccione, F. *The Theory of Open Quantum Systems*, Vol. 9780199213900, 1–656 (Oxford University Press, 2007).
- Clerk, A. A., Devoret, M. H., Girvin, S. M., Marquardt, F. & Schoelkopf, R. J. Introduction to quantum noise, measurement and amplification. *Rev. Mod. Phys.* **82**, 1155 (2008).
- Lidar, D. A. Lecture notes on the theory of open quantum systems. Preprint at <https://arxiv.org/abs/1902.00967> (2019).
- Krantz, P. et al. A quantum engineer's guide to superconducting qubits. *Appl. Phys. Rev.* **6**, 1 (2019).
- Kandala, A. et al. Error mitigation extends the computational reach of a noisy quantum processor. *Nature* **567**, 491 (2019).
- McArdle, S., Yuan, X. & Benjamin, S. Error-mitigated digital quantum simulation. *Phys. Rev. Lett.* **122**, 180501 (2019).
- Smart, S. E. & Mazziotti, D. A. Quantum-classical hybrid algorithm using an error-mitigating N -representability condition to compute the Mott metal-insulator transition. *Phys. Rev. A* **100**, 022517 (2019).
- Smart, S. E., Boyn, J.-N. & Mazziotti, D. A. Correlated states of benzyne on a quantum computer with an error-mitigated quantum contracted eigenvalue solver. *Phys. Rev. A* <https://arxiv.org/abs/2103.06876v2> (2021).
- Endo, S., Cai, Z., Benjamin, S. C. & Yuan, X. Hybrid quantum-classical algorithms and quantum error mitigation. Preprint at <https://journals.jps.jp/doi/10.7566/JPSJ.90.032001> (2020).
- Head-Marsden, K. & Mazziotti, D. A. Ensemble of Lindblad's trajectories for non-Markovian dynamics. *Phys. Rev. A* **99**, <https://doi.org/10.1103/physreva.99.022109> (2019).
- Mohseni, M. & Lidar, D. A. Direct characterization of quantum dynamics: general theory. *Phys. Rev. A* **75**, 1 (2007).
- Mohseni, M., Rezaekhani, A. T. & Lidar, D. A. Quantum-process tomography: resource analysis of different strategies. *Phys. Rev. A* **77**, 1 (2008).
- Wu, Z., Li, S., Zheng, W., Peng, X. & Feng, M. Experimental demonstration of simplified quantum process tomography. *J. Chem. Phys.* **138**, <https://doi.org/10.1063/1.4774119> (2013).
- Rey-De-Castro, R., Cabrera, R., Bondar, D. I. & Rabitz, H. Time-resolved quantum process tomography using Hamiltonian-encoding and observable-decoding. *New J. Phys.* **15**, <https://doi.org/10.1088/1367-2630/15/2/025032> (2013).
- Knill, E. et al. Randomized benchmarking of quantum gates. *Phys. Rev. A* **77**, 1 (2008).
- Blume-Kohout, R. et al. Robust, self-consistent, closed-form tomography of quantum logic gates on a trapped ion qubit. Preprint at <https://arxiv.org/abs/1310.4492> (2013).
- Nielsen, E. et al. Gate set tomography. *Quantum* **5**, 557 (2021).
- Xiang, L. et al. Quantify the non-Markovian process with intervening projections in a superconducting processor. Preprint at <https://arxiv.org/abs/2105.03333> (2021).
- White, G. A., Hill, C. D., Pollock, F. A., Hollenberg, L. C. & Modi, K. Demonstration of non-Markovian process characterisation and control on a quantum processor. *Nat. Commun.* **11**, 6301 (2020).
- Mohseni, M., Rezaekhani, A. T. & Aspuru-Guzik, A. Direct estimation of single- and two-qubit Hamiltonians and relaxation rates. *Phys. Rev. A* **77**, 1 (2008).
- Devitt, S. J., Cole, J. H. & Hollenberg, L. C. Scheme for direct measurement of a general two-qubit Hamiltonian. *Phys. Rev. A* **73**, 1 (2006).
- Head-Marsden, K., Krastanov, S., Mazziotti, D. A. & Narang, P. Capturing non-Markovian dynamics on near-term quantum computers. *Phys. Rev. Res.* **3**, 013182 (2021).
- Rost, B. et al. Simulation of thermal relaxation in spin chemistry systems on a quantum computer using inherent qubit decoherence. Preprint at <https://arxiv.org/abs/2001.00794> (2020).
- Tseng, C. H. et al. Quantum simulation with natural decoherence. *Phys. Rev. A* **62**, <https://doi.org/10.1103/physreva.62.032309> (2000).
- Bacon, D. et al. Universal simulation of markovian quantum dynamics. *Phys. Rev. A* **64**, <https://doi.org/10.1103/physreva.64.062302> (2001).
- Wang, H., Ashhab, S. & Nori, F. Quantum algorithm for simulating the dynamics of an open quantum system. *Phys. Rev. A* **83**, <https://doi.org/10.1103/physreva.83.062317> (2011).
- Sweke, R., Sinayskiy, I., Bernard, D. & Petruccione, F. Universal simulation of markovian open quantum systems. *Phys. Rev. A* **91**, <https://doi.org/10.1103/physreva.91.062308> (2015).
- Endo, S., Sun, J., Li, Y., Benjamin, S. C. & Yuan, X. Variational quantum simulation of general processes. *Phys. Rev. Lett.* **125**, <https://doi.org/10.1103/physrevlett.125.010501> (2020).
- Hu, Z., Head-Marsden, K., Mazziotti, D. A., Narang, P. & Kais, S. A general quantum algorithm for open quantum dynamics demonstrated with the Fenna-Matthews-Olson complex. Preprint at <https://arxiv.org/abs/2101.05287> (2021).
- Head-Marsden, K., Krastanov, S., Mazziotti, D. A. & Narang, P. Capturing non-Markovian dynamics on near-term quantum computers. *Phys. Rev. Res.* **3**, <https://doi.org/10.1103/physrevresearch.3.013182> (2021).
- Kamakari, H., Sun, S.-N., Motta, M. & Minnich, A. J. Digital quantum simulation of open quantum systems using quantum imaginary time evolution. Preprint at <https://arxiv.org/abs/2104.07823> (2021).
- Head-Marsden, K. & Mazziotti, D. A. Satisfying fermionic statistics in the modeling of non-Markovian dynamics with one-electron reduced density matrices. *J. Chem. Phys.* **151**, <https://doi.org/10.1063/1.5100143> (2019).
- Yoshihara, F. et al. Flux qubit noise spectroscopy using Rabi oscillations under strong driving conditions. *Phys. Rev. B* **89**, 1 (2014).
- Norris, L. M., Paz-Silva, G. A. & Viola, L. Qubit noise spectroscopy for non-Gaussian dephasing environments. *Phys. Rev. Lett.* **116**, 1 (2016).
- Yan, F. et al. Rotating-frame relaxation as a noise spectrum analyser of a superconducting qubit undergoing driven evolution. *Nat. Commun.* **4**, 2337 (2013).

46. Yu, C. C. Why study noise due to two level systems: a suggestion for experimentalists. *J. Low Temp. Phys.* **137**, 251 (2004).
47. Klimov, P. V. et al. Fluctuations of energy-relaxation times in superconducting qubits. *Phys. Rev. Lett.* **121**, 90502 (2018).
48. Niu, M. Y. et al. Learning non-Markovian quantum noise from Moiré-enhanced swap spectroscopy with deep evolutionary algorithm. Preprint at <https://arxiv.org/abs/1912.04368> (2019).
49. Schoelkopf, R. J., Clerk, A. A., Girvin, S. M., Lehnert, K. W. & Devoret, M. H. in *Quantum Noise in Mesoscopic Physics* 175–203 (2003).
50. Ithier, G. et al. Decoherence in a superconducting quantum bit circuit. *Phys. Rev. B* **72**, 134519 (2005).
51. Bylander, J. et al. Noise spectroscopy through dynamical decoupling with a superconducting flux qubit. *Nat. Phys.* **7**, 565 (2011).
52. Tokmakoff, A. Time-dependent quantum mechanics and spectroscopy. <http://tdqms.uchicago.edu/> (2014).
53. McKay, D. C. et al. Qiskit backend specifications for OpenQASM and OpenPulse experiments. Preprint at <https://arxiv.org/abs/1809.03452> (2018).
54. Kandala, A. et al. Error mitigation extends the computational reach of a noisy quantum processor. *Nature* **567**, 491 (2019).
55. Koch, J. et al. Charge-insensitive qubit design derived from the Cooper pair box. *Phys. Rev. A* **76**, 042319 (2007).
56. Chow, J. M. et al. Simple all-microwave entangling gate for fixed-frequency superconducting qubits. *Phys. Rev. Lett.* **107**, 080502 (2011).
57. Abraham, H. et al. Qiskit: an open-source framework for quantum computing. <https://doi.org/10.5281/zenodo.2562110> (2019).

Acknowledgements

We acknowledge the financial support from the U.S. Department of Energy (Office of Basic Energy Sciences) under Award No. DE-SC0019215. D. A. M. and S. K. also acknowledge the support of the National Science Foundation under award numbers CHE-1565638, CHE-2035876, DMR-2037783, and CHE-1955907. The views expressed are of the authors and do not reflect the official policy or position of IBM or the IBM Q team.

Competing interests

The authors declare no competing interests.

Additional information

Supplementary information The online version contains supplementary material available at <https://doi.org/10.1038/s42005-022-00803-8>.

Correspondence and requests for materials should be addressed to David A. Mazziotti.

Peer review information *Communications Physics* thanks the anonymous reviewers for their contribution to the peer review of this work.

Reprints and permission information is available at <http://www.nature.com/reprints>

Publisher's note Springer Nature remains neutral with regard to jurisdictional claims in published maps and institutional affiliations.



Open Access This article is licensed under a Creative Commons Attribution 4.0 International License, which permits use, sharing, adaptation, distribution and reproduction in any medium or format, as long as you give appropriate credit to the original author(s) and the source, provide a link to the Creative Commons license, and indicate if changes were made. The images or other third party material in this article are included in the article's Creative Commons license, unless indicated otherwise in a credit line to the material. If material is not included in the article's Creative Commons license and your intended use is not permitted by statutory regulation or exceeds the permitted use, you will need to obtain permission directly from the copyright holder. To view a copy of this license, visit <http://creativecommons.org/licenses/by/4.0/>.

© The Author(s) 2022, corrected publication 2022